# Tuning the Diiron Core Geometry in Carboxylate-Bridged Macrocyclic Model Complexes Affects Their Redox Properties and Supports Oxidation Chemistry

Fang Wang,[†] Sabine Becker,[†] Mikael A. Minier,[†] Andrei Loas,[†] Megan N. Jackson,[†] and Stephen J. Lippard*,[†]

[†]Department of Chemistry, Massachusetts Institute of Technology, Cambridge, Massachusetts 02139, United States

S Supporting Information

ABSTRACT: We introduce a novel platform to mimic the coordination environment of carboxylate-bridged diiron proteins by tethering a small, dangling internal carboxylate, $(CH_2)_nCOOH$, to phenol-imine macrocyclic ligands ($H_3PIMICn$). In the presence of an external bulky carboxylic acid (RCO_2H), the ligands react with $[Fe_2(Mes)_4]$ (Mes = 2,4,6-trimethylphenyl) to afford dinuclear $[Fe_2(PIMICn)-(RCO_2)(MeCN)]$ ($n = 4-6$) complexes. X-ray diffraction studies revealed structural similarities between these complexes and the reduced diiron active sites of proteins such as Class I ribonucleotide reductase (RNR) R2 and soluble methane monooxygenase hydroxylase. The number of CH_2 units of the internal carboxylate arm controls the diiron core geometry, affecting in turn the anodic peak potential of the complexes. As functional synthetic models, these complexes facilitate the oxidation of C−H bonds in the presence of peroxides and oxo transfer from O_2 to an internal phosphine moiety.
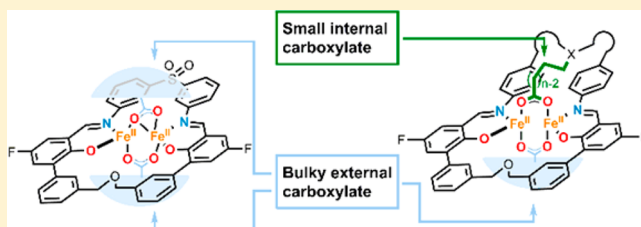
INTRODUCTION

Carboxylate-bridged diiron proteins are ubiquitous in biology. Soluble methane monooxygenase (sMMO) from methanotrophic bacteria converts C−H into C−OH bonds using dioxygen (O_2).[1,2] In this enzyme, O_2 activation and C−H bond functionalization take place at the diiron active site of the hydroxylase component (sMMOH). The reduced form of sMMOH (sMMOH$_{red}$) contains a diiron(II) core coordinated by two bridging and two terminal glutamate and two histidine residues, the latter in a *syn* configuration with respect to the Fe⋯Fe vector.[3] Class I ribonucleotide reductase (RNR) is responsible for the catalytic conversion of nucleotides to deoxynucleotides.[4,5] In its reduced form, the R2 subunit of this enzyme contains a diiron(II) site in which two glutamate residues bridge two iron atoms in a μ-1,3 binding mode.[6,7] Even though much progress has been made in modeling the active sites of these and related proteins,[8] robust complexes mimicking both structural and functional properties are rare. Because of their kinetic lability, iron carboxylate complexes tend to form polymeric species in the absence of sufficient kinetic stabilization by the ligand framework.[9,10] In addition to using multidentate ligands with simple carboxylates,[11] the desired dinuclearity could also be achieved with the use of bulky carboxylate ligands and/or a macrocyclic ligand framework. We previously employed the latter tactic using phenol-imine macrocycles (H_2PIM and H_2F_2PIM, Figure 1) together with two bulky external carboxylates (RCO_2^-).[12,13] The diiron(II) complexes of these ligands not only provide the
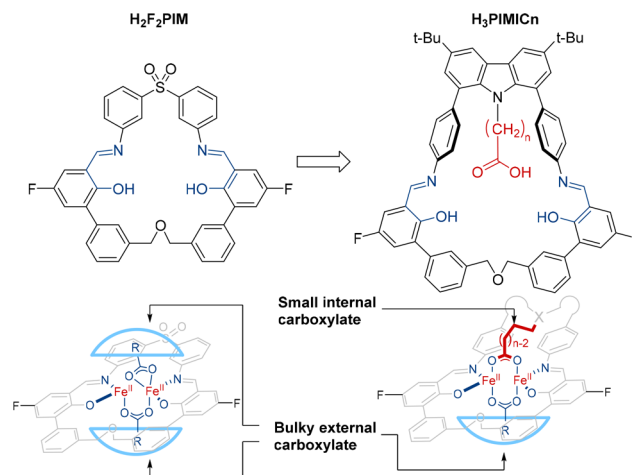
desired dinuclearity but also orient the two N-donors in a *syn* fashion with respect to the Fe⋯Fe vector.

Although these systems provide structural features characteristic of sMMOH$_{red}$, steric congestion introduced by the external carboxylate groups can impede the desired oxidation chemistry by hindering substrate access to the diiron core (Figure 1).[12] To circumvent this problem, we designed a new class of


Figure 1. Comparison of H_2F_2PIM with $H_3PIMICn$ and their diiron(II) complexes.

phenol-imine ligands in which an internal carboxylate ligand is tethered to the macrocyclic framework (H$_3$PIMICn, Figure 1). The covalent attachment of the small carboxylic acid side chain provides for the entry of potential substrates, while maintaining sufficient preorganization to prevent undesired polymerization reactions.

■ RESULTS AND DISCUSSION

Synthesis. Installation of the internal carboxylate ligand was achieved by incorporating a carbazole motif into the ligand framework. This building block is not only readily available but also provides structural features that favor orienting the appended internal carboxylate chain toward the diiron center. 3,6-Di-*tert*-butyl-1,8-bis(4-nitrophenyl)-9*H*-carbazole (**2**) was prepared by Suzuki coupling between **1**[14] and 4-nitro-phenylboronic acid pinacol ester (Scheme 1).[15] The carboxylic

Scheme 1. Synthesis[a] of [Fe$_2$(PIMICn)(RCO$_2$)(MeCN)] (*n* = 4−6) and [Fe$_2$(PIMIC3)(RCO$_2$)(MeCN)]$_2$
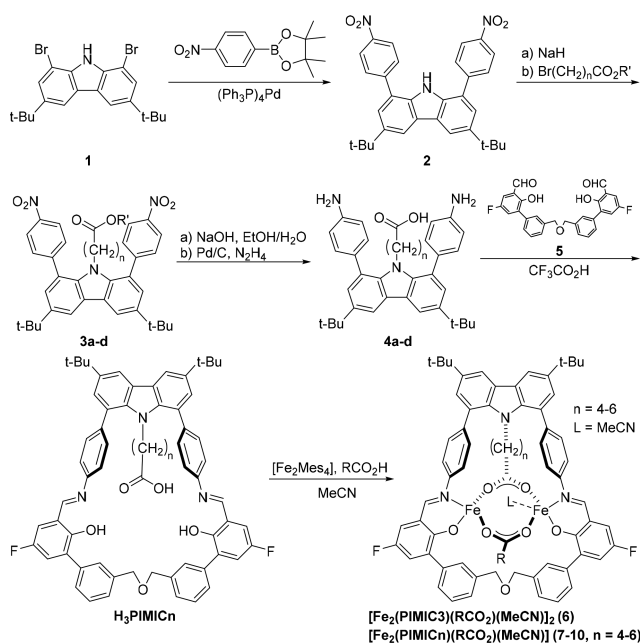
[a]See Supporting Information for experimental procedures and characterization of the ligands.

acid side chain was attached by deprotonation of **2**, followed by alkylation with the corresponding brominated carboxylic ester. Compounds **3a−d** were hydrolyzed to the carboxylic acids and then reduced by Pd-catalyzed hydrogenation with N$_2$H$_4$. The desired H$_3$PIMICn (*n* = 3−6) ligands were obtained by the cyclization reaction of **4a−d** with dialdehyde **5**. The iron complexes **6−10** were synthesized by metalating H$_3$PIMICn with [Fe$_2$Mes$_4$][16] in the presence of an external carboxylic acid (Scheme 1).

X-ray Crystallography. Single crystals of **6−10** were obtained by layering their solutions in toluene, tetrahydrofuran (THF), or CH$_2$Cl$_2$ with MeCN. Unexpectedly, upon metalation of H$_3$PIMIC3 in the presence of 9-anthracenecarboxylic acid (AnthCO$_2$H), the tetranuclear [Fe$_2$(PIMIC3)(AnthCO$_2$)-(MeCN)]$_2$ (**6**) was obtained (see Table S1 and Figure S1 in the Supporting Information). The crystal structure of **6** revealed that the two PIMIC3 ligands orient in a head-to-tail mode through binding of the internal carboxylate of one ligand

to the diiron center of the other (Figure 2a). A closer inspection of the structure suggests this undesired higher
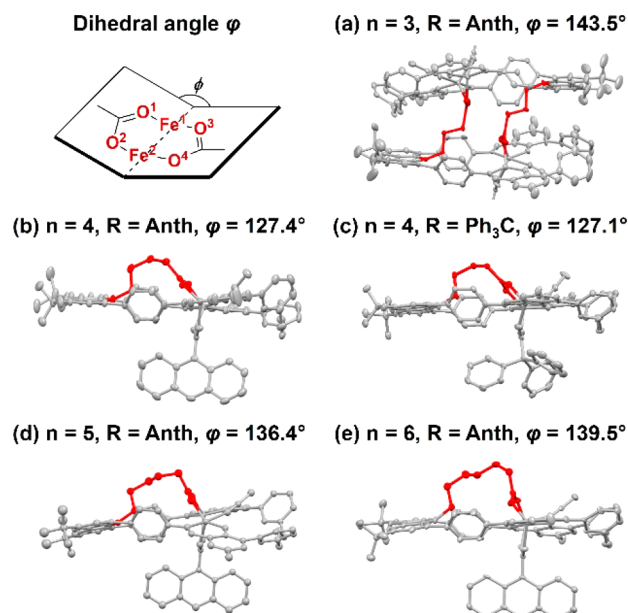
Figure 2. Dihedral angle (φ) between the internal and external carboxylate groups of the iron(II) complexes [Fe$_2$(PIMIC3)-(AnthCO$_2$)(MeCN)]$_2$ and [Fe$_2$(PIMICn)(RCO$_2$)(MeCN)] (*n* = 4−6). (a−e) Molecular structures of **6−10** in ORTEP representations with thermal ellipsoids set at 50% probability. Atoms of the internal carboxylate arms are highlighted in red. All other atoms are colored in gray. H atoms and solvent molecules were omitted for clarity. See Supporting Information for complete crystallographic data.

nuclearity is a result of the internal carboxylate chain being too short to allow for intramolecular coordination. Consistent with this idea, we discovered that H$_3$PIMIC4, containing a longer (CH$_2$)$_4$CO$_2$H chain, favors formation of dinuclear complexes **7** and **8** with anthracene and trityl carboxylate donors, respectively. Crystallographic studies confirmed that both complexes have the desired dinuclearity and almost identical diiron core geometries (Figure 2b,c). Thus, the external carboxylates exert limited influence on the geometry of the diiron center in PIMICn-based complexes.

As depicted in Figure 3, both internal and external carboxylates bind to the diiron center in the μ-1,3 mode, differing from the μ-1,3 and the μ-η^1:η^2 carboxylate bridges observed in PIM-based diiron(II) analogues[12,13] and sMMOH$_{red}$.[3] The Fe−O and Fe−N bond distances of the diiron core structures in **7** and **8** are very similar to those of [Fe$_2$(PIM)(RCO$_2$)$_2$] and [Fe$_2$(F$_2$PIM)(RCO$_2$)$_2$]. The longer Fe···Fe distances of 3.90−4.07 Å in the PIMIC-based complexes, compared with those in [Fe$_2$(PIM)(RCO$_2$)$_2$] and [Fe$_2$(F$_2$PIM)(RCO$_2$)$_2$] (3.56−3.64 Å), may reflect the slightly wider opening of the two phenol-imine binding motifs of PIMIC, further supported by the longer N···N distances of 7.26−7.51 versus 6.36−6.58 Å, respectively. The asymmetric μ-η^1:η^2 carboxylate bridging mode in [Fe$_2$(PIM)(RCO$_2$)$_2$] and [Fe$_2$(F$_2$PIM)(RCO$_2$)$_2$] also contributes to the shorter Fe···Fe distances observed in these complexes. Overall, the diiron core structure of [Fe$_2$(PIMIC4)(RCO$_2$)(MeCN)] is geometrically analogous to that of sMMOH$_{red}$ in terms of the *syn* orientation of the N donors. The two μ-1,3 bridging carboxylates and an Fe···Fe distance of ca. 3.9 Å in complexes
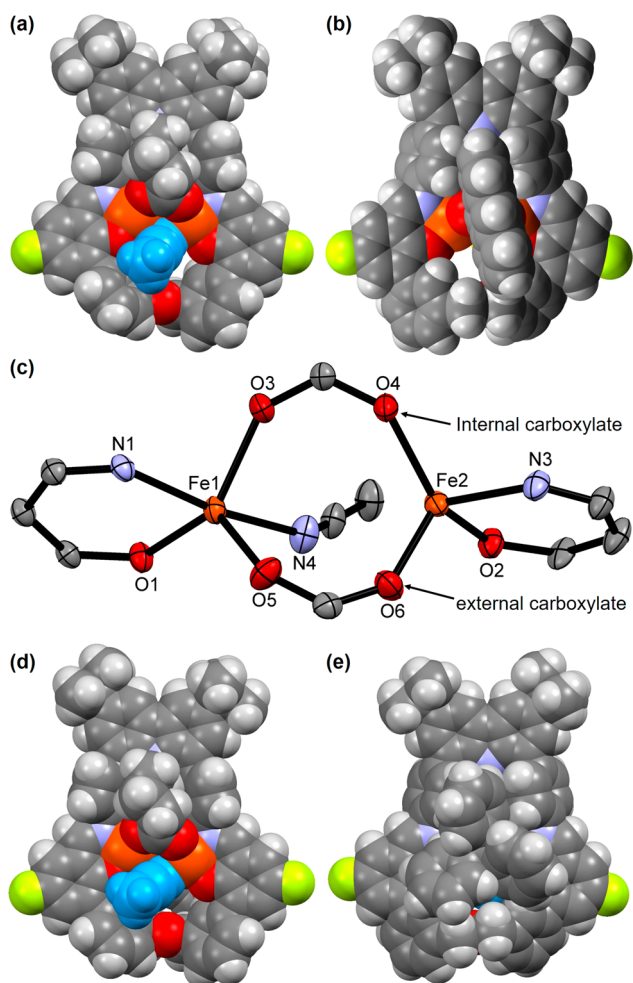
Figure 3. Molecular structures of $[Fe_2(PIMIC4)(AnthCO_2)(MeCN)]$ (**7**) and $[Fe_2(PIMIC4)(Ph_3CCO_2)(MeCN)]$ (**8**). (a) Space-filling view of **7** from the internal carboxylate side. (b) Space-filling view of **7** from the external carboxylate side. (c) Diiron core of **7** in ORTEP representation with thermal ellipsoids set at 50% probability. Color scheme: iron, orange; carbon, gray; nitrogen, blue; oxygen, red; fluorine, yellow; MeCN (a, d), light blue. Selected distances (Å) and bond angles (deg): Fe(1)···Fe(2) = 3.972(1); Fe(1)−O(1) = 1.9335(18); Fe(1)−O(3) = 2.019(2); Fe(1)−O(5) = 2.022(2); Fe(1)−N(1) = 2.140(2); Fe(1)−N(4) = 2.261(3); Fe(2)−O(2) = 1.9163(19); Fe(2)−O(4) = 1.991(2); Fe(2)−O(6) = 1.983(2); Fe(2)−N(3) = 2.067(2); Fe(2)−N(4) = 2.887(3); O(3)−Fe(1)−O(5) = 105.13(9); O(1)−Fe(1)−N(1) = 86.40(8); O(4)−Fe(2)−O(6) = 109.67(9); O(2)−Fe(2)−N(3) = 89.45(9). (c) H atoms were omitted for clarity. See Table S1 in the Supporting Information for complete crystallographic data. (d) Space-filling view of **8** from the internal carboxylate side. (e) Space-filling view of **8** from the external carboxylate side.

7 and **8**, however, closely mimic the active site of the reduced Class I RNR R2 protein.[6,7] The covalently tethered internal carboxylate chains in **7** and **8** presumably confer a higher degree of preorganization than external carboxylates. Therefore, dinuclearity is preferred by **7** and **8**. In contrast, small *external* carboxylate ligands lack the preorganization conveyed by tethering and typically produce polynuclear complexes.[9,10] As anticipated, MeCN resides in the diiron binding pocket on the side of the internal carboxylate chain, which is the more sterically accessible position. Space-filling views of $[Fe_2(PIMIC4)(AnthCO_2)(MeCN)]$ and $[Fe_2(PIMIC4)-$

$(Ph_3CCO_2)(MeCN)]$ show similar substrate accessibility to the diiron core from the internal carboxylate side (Figure 3a,d).

In addition to **7** and **8**, diiron complexes of H$_3$PIMIC5 and H$_3$PIMIC6 with AnthCO$_2^-$ as an external carboxylate were also prepared (**9** and **10**, Scheme 1). Their crystal structures reveal that, in the solid state, the diiron core geometry is essentially the same as that encountered in **7** and **8**. In particular, the Fe···Fe distances in **9** and **10** range from 3.9 to 4.1 Å, values also observed in **7** and **8**. Although the diiron(II) complexes **6**−**10** share many structural features, they differ in the dihedral angle (φ) between the internal and external carboxylate groups, defined as the angle between least-squares mean planes O^1−Fe^1−Fe^2−O^2 and O^3−Fe^1−Fe^2−O^4 (Figure 2). With the exception of dimeric $[Fe_2(PIMIC3)(AnthCO_2)(MeCN)]_2$ (**6**), in which the carboxylate chain from one ligand binds to the diiron center of the other ligand framework, φ increases with the length of the carboxylate chain. Importantly, φ values for **7** and **8** are almost identical, further supporting the limited impact of the external carboxylate on the core geometry of the complexes. To test whether the nuclearity of the iron species is affected by the presence of coordinating solvents, the dichloromethane-containing analogue of **10**, $[Fe_2(PIMIC6)-(AnthCO_2)]\cdot CH_2Cl_2$ (**11**), was isolated by layering a toluene−CH$_2$Cl$_2$ solution of the complex with pentane. Compound **11** retained the structure of the diiron(II) complex **10**, indicating that nuclearity is independent of the cocrystallized solvent (see Figure S7 and Table S2 in the Supporting Information for complete crystallographic data).

Electrochemistry. To investigate whether the redox properties of the diiron complexes are affected by their core geometries, cyclic voltammograms (CV) of **6**−**10** were performed in CH$_2$Cl$_2$ with (n-Bu$_4$N)PF$_6$ as supporting electrolyte and a three-electrode setup using ferrocene/ferrocenium as an internal standard. At scan rates of up to 500 mV/s, all complexes displayed redox couples with various degrees of reversibility (Figures 4a and S15−S19). The degree
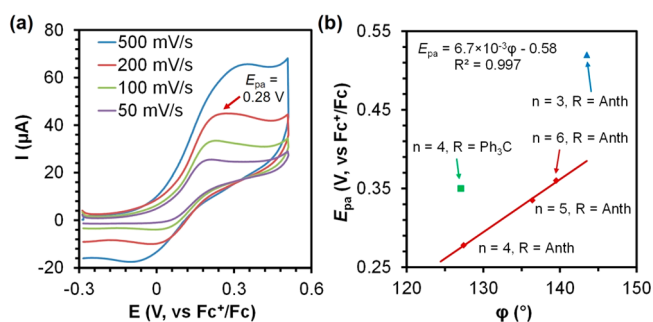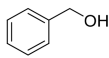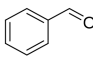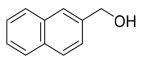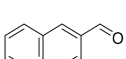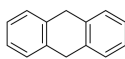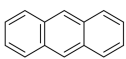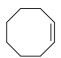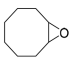

Figure 4. (a) CVs of 1.0 mM solutions of **7** in CH$_2$Cl$_2$ at various scan rates. (b) Linear relationship between φ and anodic peak potentials (E_{pa}) of the iron(II) complexes $[Fe_2(PIMICn)(RCO_2)(MeCN)]$ (n = 4−6). The E_{pa} values determined for **6**−**10** at scan rate of 200 mV/s are 0.52, 0.28, 0.35, 0.34, and 0.36 V vs Fc$^+$/Fc, respectively.

of reversibility does not appear to be significantly affected by solvent polarity, as observed in the case of **7** in dichloromethane−acetonitrile mixtures (Figure S16E).

In carboxylate-bridged diiron complexes, if the Fe centers are electronically coupled through the carboxylate bridge, the second Fe center is oxidized at potentials more positive than the first, and two one-electron redox features are observed in CVs. If, however, there is little or no electronic coupling, the Fe centers are oxidized at identical or nearly identical potentials,

Table 1. Oxidation Reactions Facilitated by the $[Fe_2(PIMIC4)(AnthCO_2)(MeCN)]$-$CO(NH_2)_2 \cdot H_2O_2$ System

$$\text{iron-containing compound} \; + \; \text{substrate} \; + \; \text{urea-}H_2O_2 \; \xrightarrow[\text{0.5 h}]{CH_2Cl_2, \text{ r.t.}} \; \text{product}$$

| | | | | 1.0 equiv. | 5.0 equiv. |

entry	substrate	BDE_{C-H} (kcal/mol)	product	conv. with 7[a]	conv. with iron(II) triflate [b]	conv. with urea-H_2O_2 only [c]
1	(benzyl alcohol)	82.6	(benzaldehyde)	21%	12%[d]	trace
2	(2-hydroxymethylnaphthalene)	76.6	(2-naphthaldehyde)	49%	2%[d]	trace
3	(dihydroanthracene)	78.0	(anthracene)	18%	14%	trace
4	Ph_3CH	81.0	Ph_3COH	-[e]	-[e]	-[e]
5	(cyclooctene)	-	(cyclooctene oxide)	-[e]	-[e]	-[e]

[a]Conversion of substrate in the presence of 1.0 equiv of $[Fe_2(PIMIC4)(AnthCO_2)(MeCN)]$ (**7**). [b]Conversion of substrate in the presence of 2.0 equiv of $[Fe(OTf)_2(MeCN)_2]$. [c]Conversion of substrate in the absence of iron-containing compounds. [d]In the presence of $[Fe(OTf)_2(MeCN)_2]$, the reason for the higher conversion of benzyl alcohol vs 2-hydroxymethylnaphthalene is unclear. [e]No product was detected by gas chromatography–mass spectrometry.

and a two-electron redox wave is observed.[17,18] Several homonuclear dimetallic complexes have similar two-electron redox features that are assigned as two sequential one-electron transfers occurring at nearly identical potentials.[19,20] In RNR R2, the lack of an observable Fe(II)Fe(III) valence state has been attributed to the first electron transfer occurring at a more negative potential than the second.[21]

The CV of **7** shows two oxidation events at 0.12 and 0.44 V (Figure S20). The H_3PIMIC4 ligand on its own shows a redox feature at 0.77 V (Figure S20), so we attribute both of the redox features observed in **7** to Fe-based oxidations rather than ligand oxidation. Bulk electrolysis of **7** at 0.17 V gave 1.5 and 1.9 electrons per molecule (Figures S20A−D), suggesting that the first wave is a two-electron oxidation event. Complex **7**, however, decomposes rapidly upon oxidation (Figures S20F,G). Therefore, on the basis of the fact that there are two metal-based redox features in the CVs, it is likely that the waves at 0.12 and 0.44 V correspond to the Fe(II)Fe(II) → Fe(II)Fe(III) and Fe(II)Fe(III) → Fe(III)Fe(III) processes, respectively. The decomposition of the oxidized compound, however, prevents further spectroscopic characterization, so we cannot unequivocally assign it an oxidation state.

As shown in Figure 4b, the anodic peak potentials (E_{pa}, vs Fc$^+$/Fc) of complexes **7−9** linearly increase with φ over the +0.28 to +0.36 V range (R^2 = 0.997). Varying the length of the $(CH_2)_n$ arm does not alter the electronic properties of the internal carboxylate, the Fe···Fe distances, Fe−O/N bond distances, or the nuclearity of **7−9**. Therefore, we attribute the differences in E_{pa} values for complexes **7−9** mainly to variations in φ. This result implies that, apart from protein−protein interactions,[22,23] conformational changes in the diiron core geometry may also tune the redox potential and, presumably, the reactivity of carboxylate-bridged diiron centers in metalloproteins. Substituting the external AnthCO_2$^−$ bridging ligand in **7** with Ph_3CCO_2$^−$ in **8** induces a variation of +0.07 V in E_{pa}. On the basis of the pK_a values of AnthCO_2H and Ph_3CCO_2H

in aqueous solutions, 3.65[24] and 3.96,[25] respectively, their carboxylate groups should have similar electronic properties. Thus, the electrochemical data suggest that the steric properties of the carboxylate ligands may also affect the E_{pa} values. A comparison of tetranuclear **6** (E_{pa} = 0.52 V) and dinuclear **10** (E_{pa} = 0.36 V) reveals that other factors, such as steric shielding of the diiron core induced by higher nuclearity, can influence the anodic peak potential.

A remaining question is whether the observed correlation could be explained on theoretical grounds. Even though density functional theory (DFT) calculations have been used to predict the redox potential of electrochemically active metal complexes, routine computational methods are typically prone to errors of ~150 mV and thus may not be suitable for rationalizing the ~240 mV changes in E_{pa} observed in this work.[26,27] In addition to the limitations of the theoretical calculations, the conformation of the internal carboxylate arm determined in the solid state may not necessarily reflect the structure in the electrolyte-containing solution used for electrochemical studies. Lastly, we cannot rule out the possibility of the correlation of Figure 4b being coincidental. For all these reasons, we refrain here from providing conclusive rationales regarding this correlation. More investigations may be of interest for future studies.
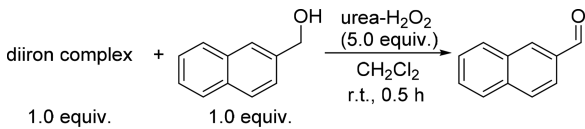
Oxidation Chemistry. A fundamental goal in devising synthetic mimics of diiron protein active sites is to replicate their functionality.[28,29] To explore the reactivity of the new PIMIC-based complexes toward oxidants, **7** was initially treated with excess O_2, urea-hydrogen peroxide ($CO(NH_2)_2 \cdot H_2O_2$), or 2-methyl-1-phenylprop-2-yl hydroperoxide (MPPH) in CH_2Cl_2 at room temperature. An immediate color change from red to dark brown was observed. Layering the reaction mixture of **7** and MPPH in CH_2Cl_2 with MeCN afforded two types of X-ray quality crystals, namely, dark brown rectangular blocks and brown needles. Crystallographic studies revealed the rectangular blocks and the brown needles to be the triiron

[Fe₃O(HPIMIC4)₂(AnthCO₂)₂(MeCN)] (**12**) and tetrairon [Fe₄(μ-O)₂(μ-HO)₂(PIMIC4)₂] (**13**) species, respectively (see Figures S8 and S9 for structural details and Table S5 for oxidation state assignment). This result can be ascribed to insufficient preorganization imparted by the PIMIC4 ligand and is similar to previous observations for [Fe₂(PIM)(Ph₃CCO₂)₂], which reacts with O₂ to give diiron [Fe₂(μ−OH)(PIM)(Ph₃CCO₂)₃] and tetrairon [Fe₄(μ−OH)₆(PIM)₂(Ph₃CCO₂)₂] complexes.[12]

We further investigated whether PIMIC4-based diiron complexes facilitate substrate oxidation. In the presence of O₂, [Fe₂(PIMIC4)(AnthCO₂)(MeCN)] (**7**) does not promote the oxidation of triphenylphosphine, benzyl alcohol, 2-hydroxymethylnaphthalene, or dihydroanthracene (DHA) in CH₂Cl₂ at room temperature. In contrast, in the presence of **7** and CO(NH₂)₂·H₂O₂ as the oxidant, benzyl alcohol underwent oxidation to benzaldehyde with 21% conversion (Table 1, entry 1 and Figure S21). The oxidation also occurred in the presence of [Fe(OTf)₂(MeCN)₂], albeit with a lower conversion (12%), indicating a modest effect of **7** on the transformation (Table 1, entry 1 and Figure S21). Having weaker methylene C−H bonds,[30,31] 2-hydroxymethylnaphthalene was oxidized to the corresponding aldehyde with a significantly higher conversion (Table 1, entry 2 and Figure S22). Although DHA also has weak methylene C−H bonds, **7** was not significantly more effective than [Fe(OTf)₂(MeCN)₂] in terms of its ability to facilitate the oxidation (Table 1, entry 3 and Figure S23). This result might reflect the more facile oxidation of the O−H bond, which initiates the oxidation of alcohols, than the C−H bond.[32] For similar reasons, anthrone, which can tautomerize to 9-hydroxyanthracene, is more reactive than DHA in oxidation reactions promoted by dendrimer-based carboxylate-rich diiron complexes.[33] Triphenylmethane was not converted to triphenylmethanol (Table 1, entry 4), whereas *cis*-cyclooctene was inert under the current reaction conditions (Table 1, entry 5).

To evaluate the influence of the steric bulk of the external carboxylate ligands on the activity of diiron complexes, [Fe₂(F₂PIM)(AnthCO₂)₂(THF)] (**14**) and [Fe₂(F₂PIM)(Ph₃CCO₂)₂] (**15**) were synthesized (see Supporting Information for details). X-ray diffraction studies showed that the diiron cores of these complexes have essentially the same structural features as those previously described for PIM- or F₂PIM-based diiron(II) complexes.[12,13] On the basis of the size and the number of external carboxylate ligands in the complexes, the accessibility of guest molecules to the diiron center can be ranked as [Fe₂(PIMIC4)(RCO₂)(MeCN)] (**7**, **8**) > [Fe₂(F₂PIM)(AnthCO₂)₂(THF)] (**14**) > [Fe₂(F₂PIM)(Ph₃CCO₂)₂] (**15**) (Figures 1 and 3). The presence of coordinating THF in **14**, crystallized from a solution in CH₂Cl₂, THF, and pentane, may not necessarily indicate a more accessible diiron center in **14** than those in **7** and **8**. The absence of THF in **7** and **8**, crystallized from a mixture of MeCN and THF, is more likely due to the stronger coordinating ability of MeCN compared to THF.[34] We further explored the oxidation of 2-hydroxymethylnaphthalene in the presence of these complexes (Table 2 and Figure S24). Both PIMIC-based complexes show essentially the same activity. Despite a more restricted substrate accessibility to the diiron core of **14** and **15** due to the two bulky external carboxylates, these complexes exhibit higher substrate conversions than those of **7** and **8**. This observation does not support the initially

Table 2. Oxidation of 2-Hydroxymethylnaphthalene with Urea-H₂O₂ in the Presence of Different Diiron Complexes

diiron complex	conv[a]
[Fe₂(PIMIC4)(AnthCO₂)(MeCN)] (**7**)	49%
[Fe₂(PIMIC4)(Ph₃CCO₂)(MeCN)] (**8**)	47%
[Fe₂(F₂PIM)(AnthCO₂)₂(THF)] (**14**)	69%
[Fe₂(F₂PIM)(Ph₃CCO₂)₂] (**15**)	59%

[a]Conversion of substrate in the presence of 1.0 equiv of diiron complex as determined by gas chromatography−mass spectrometry.

postulated role of diiron core accessibility in governing the reactivity of the complexes (Figure 1).

In addition to oxidation reactions of external substrates with peroxide, we also explored tethered substrates with the PIMIC-based diiron complexes. To study these reactions, a series of analogues containing internal reactive motifs, including phosphine, [Fe₂(PIMIC4)(o-Ph₂PC₆H₄CO₂)(MeCN)] (**16**), sulfide, [Fe₂(PIMIC4)(o-PhSC₆H₄CO₂)(MeCN)] (**17**), and benzylic C−H bonds, [Fe₂(PIMIC4)(o-Ph₂CHC₆H₄CO₂)(MeCN)] (**18**), were prepared (Figure 5). The oxidation of these functional groups has been previously reported with carboxylate-rich diiron(II) compounds.[35] Of these substrates, however, only the phosphine analogue **16** underwent oxidation, forming the corresponding phosphine oxide with 86% conversion in the presence of O₂. It was previously discovered that the efficiency of oxidizing internal sulfides of [Fe₂(μ-O₂CAr)₃(O₂CAr)(picSR)] (picSR = *ortho*-substituted picolyl-based ligands) closely depends on the Fe···S distances.[35] By oxidizing a complex having an Fe···S distance of 4.03 Å, sulfoxide was obtained in only 38% yield. The significantly longer Fe···S distances (4.826−4.911 Å) in [Fe₂(PIMIC4)(o-PhSC₆H₄CO₂)(MeCN)] (**17**) may account for its lack of reactivity. The reason for the inertness of **18** toward benzylic C−H oxidation is currently unknown.

We then used 2-methyl-1-phenyl-2-propyl hydroperoxide (MPPH) to differentiate homolytic versus heterolytic cleavage of the hydroperoxide O−OH bonds (Scheme 2a).[36−39] Homolytic cleavage of the O−OH bond leads to the PhCH₂C(Me)₂O· radical. This species undergoes rapid β-scission of the PhH₂**C**−**C**(Me)₂ bond to generate a benzyl radical, which can further convert to benzyl alcohol, bibenzyl, or toluene, among others (Scheme 2a). By comparison, heterolytic cleavage yields 2-methyl-1-phenylpropan-2-ol as the only byproduct, thereby distinguishing the two reaction pathways.

As shown in Scheme 2b, the reaction between **7** and MPPH in CH₂Cl₂ under anaerobic conditions affords 2-methyl-1-phenylpropan-2-ol and bibenzyl in a ratio of ∼3:1, suggesting predominant heterolytic cleavage of the O−OH bond (Figure S25). The importance of the heterolytic oxidation pathway is also evident from the oxidation of 2-hydroxymethynaphthalene in the presence of MPPH and **7** (Figure S26). Under these conditions, 2-methyl-1-phenylpropan-2-ol and bibenzyl, the byproducts of MPPH, were rendered in a 3:2 ratio. Iron-mediated O−O bond cleavage reactions involving both homolytic and heterolytic pathways have been previously described.[40−42] 2-(Allylphenyl)methanol, a bifunctional substrate, was employed to explore the preference of C−H bond
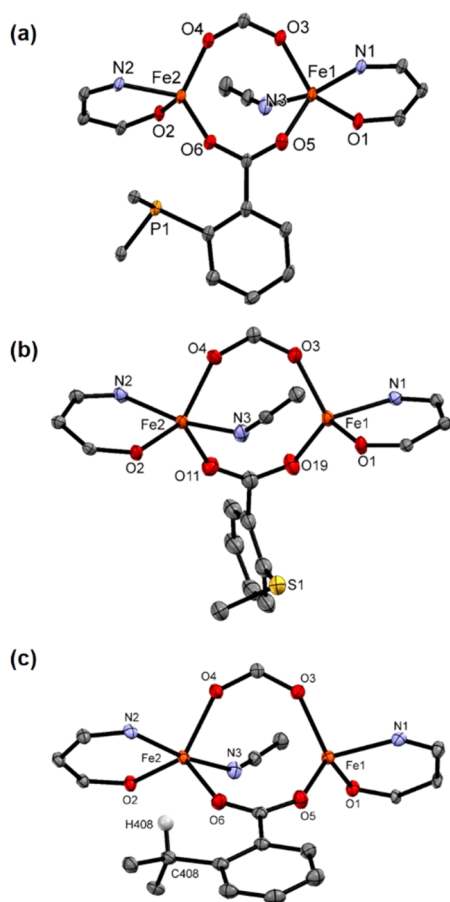
Figure 5. Views of the diiron cores in (a) [Fe$_2$(PIMIC4)(o-Ph$_2$PC$_6$H$_4$CO$_2$)(MeCN)] (**16**), (b) [Fe$_2$(PIMIC4)(o-PhSC$_6$H$_4$CO$_2$)(MeCN)] (**17**), and (c) [Fe$_2$(PIMIC4)(o-Ph$_2$CHC$_6$H$_4$CO$_2$)(MeCN)] (**18**) as ORTEP representations with thermal ellipsoids set at 50% probability. H atoms were omitted for clarity. Only *ipso* carbon atoms of the phenyl rings are shown for clarity. Color scheme: iron, orange; carbon, gray; nitrogen, blue; oxygen, red; sulfur, yellow; phosphorus, light orange. The complete X-ray crystal structures are provided in the Supporting Information.

oxidation over the oxo-transfer reaction (Scheme 2d). Upon treatment of (2-allylphenyl)methanol with **7** and urea–H$_2$O$_2$, 2-allylbenzaldehyde was the only oxidation product; epoxidation of the allyl moiety was not observed (Figure S27). This finding suggests a relatively higher reaction barrier to the oxo-transfer reaction and may explain the low reactivity of *cis*-cyclooctene (Table 1). Even though these studies provide insight into peroxide O–O bond cleavage pathways, the active iron-containing species involved in the oxidation chemistry are not elucidated. Moreover, it remains unclear whether the tri- (**12**) and tetrairon (**13**) complexes isolated in the reaction between **7** and MPPH are relevant to the substrate oxidation chemistry.

CONCLUSIONS

Diiron(II) complexes of a series of macrocyclic ligands with covalently tethered carboxylates were prepared and evaluated as synthetic models of diiron protein active sites, such as sMMOH$_{red}$ and reduced Class I RNR R2. By varying the length of the internal carboxylate arm, key features of the complexes, including the first coordination sphere environment and nuclearity, could be precisely tuned. The anodic peak
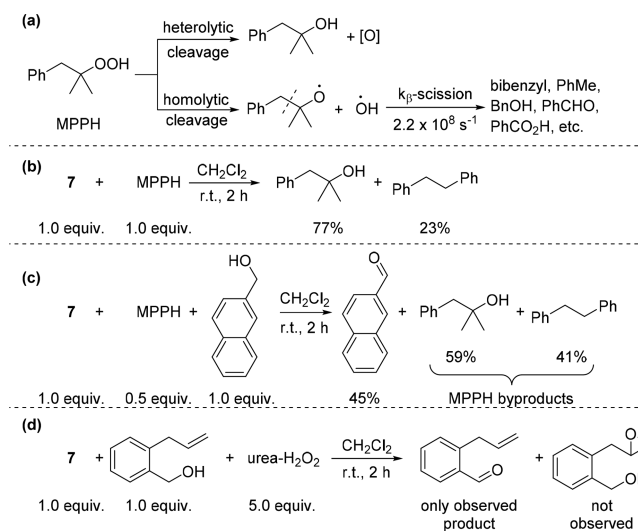
Scheme 2[a]

[a](a) Homo- and heterolytic cleavage products of MPPH. (b) Product distribution of the reaction of **7** and MPPH. (c) Product distribution of the reaction of **7**, 2-hydroxymethylnaphthalene and MPPH. (d) Product distribution of the reaction of **7**, (2-allylphenyl)methanol and urea−H$_2$O$_2$.

potential of diiron(II) compounds [Fe$_2$(PIMICn)(AnthCO$_2$)-(MeCN)], $n = 4$ to 6, increases linearly with the dihedral angle between the internal and external carboxylate groups. As functional models, these compounds facilitate C−H bond oxidation in the presence of peroxides. The accessibility of substrates to the diiron core can be controlled by pairing the internal carboxylate ligand with specific external carboxylates. Internal substrate oxidation with O$_2$ was also observed. Preliminary mechanistic studies using MPPH as an oxidant reveal both heterolytic and homolytic O−OH bond cleavage.

EXPERIMENTAL SECTION

For general procedures, methods, the synthesis of ligands and other reagents, as well as the details of the oxidation chemistry, see the Supporting Information.

[Fe$_2$(PIMIC3)(AnthCO$_2$)(MeCN)]$_2$ (6). In an anaerobic drybox, solid H$_3$PIMIC3 (39.4 mg, 40 μmol) and 9-anthracenecarboxylic acid (8.9 mg, 40 μmol) were dissolved in 1.0 mL of THF. A 1.0 mL solution of THF containing [Fe$_2$(Mes)$_4$] (23.5 mg, 40 μmol) was added to the reaction vessel, and the mixture was stirred for 1 h. The dark red solution was evaporated to dryness, and the residue was redissolved in CH$_2$Cl$_2$. The solution was filtered through a glass wool plug and layered with MeCN. Red crystals formed over several days. The solid material was collected by filtration and washed with pentane to give the desired diiron complex (44.2 mg, 81%). Crystals suitable for X-ray diffraction studies were obtained by layering a solution of the complex in toluene with MeCN. IR (KBr): ν 3049, 2954, 2898, 2863, 1597, 1579, 1545, 1445, 1424, 1337, 1281, 1181, 1000, 840, 784, 732, 533 cm^{-1}. Anal. Calcd for C$_{79}$H$_{63}$F$_2$Fe$_2$N$_3$O$_7$·(CH$_3$CN)$_{0.5}$·CH$_2$Cl$_2$: C, 68.44; H, 4.72; N, 3.45. Found: C, 68.20; H, 4.40; N, 3.18%. mp (decomp) = 262.5 °C.

[Fe$_2$(PIMIC4)(AnthCO$_2$)(MeCN)] (7). In an anaerobic drybox, solid H$_3$PIMIC6 (154.2 mg, 0.15 mmol) and 9-anthracenecarboxylic acid (33.3 mg, 0.15 mmol) were dissolved in 6.0 mL of THF. A 4.0 mL solution of THF containing [Fe$_2$(Mes)$_4$] (88.3 mg, 0.15 mmol) was added to the reaction vessel, and the mixture was stirred for 1 h. The crystallization was performed as described above for **6**. The solid material was collected by filtration and washed with pentane to give the desired diiron complex (183.7 mg, 89%). Crystals suitable for X-ray diffraction studies were obtained by layering a solution of the

complex in THF with MeCN. IR (KBr): ν 3049, 2958, 2902, 2863, 1601, 1584, 1549, 1450, 1424, 1337, 1277, 1203, 1143, 1000, 840, 788, 732, 697, 671, 533 cm^{-1}. Anal. Calcd for $C_{80}H_{65}F_2Fe_2N_3O_7 \cdot (CH_3CN)_{1.5} \cdot (CH_2Cl_2)_{2.8}$: C, 63.24; H, 4.65; N, 3.87. Found: C, 63.28; H, 4.81; N, 3.82%. mp (decomp) = 272.9 °C.

[Fe$_2$(PIMIC4)(Ph$_3$CCO$_2$)(MeCN)] (8). In an anaerobic drybox, solid H$_3$PIMIC4 (75.0 mg, 0.075 mmol) and Ph$_3$CCO$_2$H (21.6 mg, 0.075 mmol) were dissolved in 3.0 mL of THF. A 2.0 mL solution of THF containing [Fe$_2$(Mes)$_4$] (44.1 mg, 0.075 mmol) was added to the reaction vessel, and the mixture was stirred for 1 h. The crystallization was performed as described above for **6**. The solid material was collected by filtration and washed with pentane to give the desired diiron complex (91.8 mg, 85%). Crystals suitable for X-ray diffraction studies were obtained by layering a solution of the complex in THF with MeCN. IR (KBr): ν 3056, 3031, 2918, 2850, 1578, 1545, 1490, 1444, 1418, 1378, 1322, 1304, 1284, 1200, 1175, 1152, 1097, 1085, 1036, 985, 790, 745, 699, 673, 547 cm^{-1}. Anal. Calcd for $C_{85}H_{71}F_2Fe_2N_3O_7 \cdot CH_3CN \cdot CH_2Cl_2$: C, 69.44; H, 5.03; N, 3.68. Found: C, 69.71; H, 4.88; N, 3.54%. mp (decomp) = 286.5 °C.

[Fe$_2$(PIMIC5)(AnthCO$_2$)(MeCN)] (9). In an anaerobic drybox, solid H$_3$PIMIC5 (150.0 mg, 0.15 mmol) and AnthCO$_2$H (33.3 mg, 0.15 mmol) were dissolved in 6.0 mL of THF. A 5 mL solution of THF containing [Fe$_2$(Mes)$_4$] (88.3 mg, 0.15 mmol) was added to the reaction vessel, and the mixture was stirred for 1 h. The crystallization was performed as described above for **6**. The solid material was collected by filtration and washed with MeCN to give the desired diiron complex (128.0 mg, 63%). Crystals suitable for X-ray diffraction studies were obtained by layering a solution of the complex in either THF or dichloromethane with MeCN. IR (KBr): ν 3049, 2958, 2902, 2863, 1601, 1579, 1553, 1445, 1428, 1320, 1277, 1203, 1147, 996, 844, 788, 732, 697, 671, 533 cm^{-1}. Anal. Calcd for $C_{81}H_{67}F_2Fe_2N_3O_7 \cdot CH_3CN \cdot CH_2Cl_2$: C, 68.63; H, 4.94; N, 3.81. Found: C, 68.84; H, 4.89; N, 3.54%. mp (decomp) = 263.5 °C.

[Fe$_2$(PIMIC6)(AnthCO$_2$)(MeCN)] (10). In an anaerobic drybox, solid H$_3$PIMIC6 (154.2 mg, 0.15 mmol) and AnthCO$_2$H (33.3 mg, 0.15 mmol) were dissolved in 6.0 mL of THF. A 5 mL solution of THF containing [Fe$_2$(Mes)$_4$] (88.3 mg, 0.15 mmol) was added to the reaction vessel, and the mixture was stirred for 1 h. The crystallization was performed as described above for **6**. The solid material was collected by filtration and washed with MeCN to give the desired diiron complex (181.1 mg, 89%). Crystals suitable for X-ray diffraction studies were obtained by layering a solution of the complex in THF with MeCN. IR (KBr): 3049, 2954, 2902, 2859, 1597, 1579, 1549, 1445, 1424, 1316, 1281, 1203, 1143, 1000, 840, 788, 732, 697, 672, 538 cm^{-1}. Anal. Calcd for $C_{82}H_{69}F_2Fe_2N_3O_7 \cdot CH_3CN \cdot (CH_2Cl_2)_{0.5}$: C, 70.07; H, 5.09; N, 3.86. Found: C, 69.93; H, 5.08; N, 3.59%. mp (decomp) = 308.3 °C. [Fe$_2$(PIMIC6)(AnthCO$_2$)]·(CH$_2$Cl$_2$) **(11)** was obtained by layering a solution of complex in toluene and CH$_2$Cl$_2$ with pentane.

[Fe$_3$(μ_3-O)(HPIMIC$_4$)$_2$(AnthCO$_2$)$_2$(MeCN)] (12) and [Fe$_4$(μ-O)$_2$(μ-OH)$_2$(PIMIC4)$_2$] (13). In an anaerobic drybox, [Fe$_2$(PIMIC4)(AnthCO$_2$)(MeCN)] (27.4 mg, 0.020 mmol) was dissolved in anhydrous CH$_2$Cl$_2$. MPPH (3.3 mg, 0.020 mmol) was added to the reaction mixture, and a dark brown solution formed immediately. The mixture was stirred for 1 h and layered with MeCN. After 2 d, X-ray diffraction quality crystals formed as a mixture of dark brown rectangular blocks (**12**) and brown needles (**13**). The solid material was collected by filtration and washed with MeCN (13.6 mg).

[Fe$_2$(F$_2$PIM)(AnthCO$_2$)$_2$(THF)] (14). In an anaerobic drybox, solid H$_2$F$_2$PIM (69.0 mg, 0.10 mmol) and AnthCO$_2$H (44.4 mg, 0.20 mmol) were dissolved in 4.0 mL of THF. A 2.0 mL solution of THF containing [Fe$_2$(Mes)$_4$] (58.8 mg, 0.10 mmol) was added to the reaction vessel, and the mixture was stirred for 1 h. The dark red solution was evaporated to dryness, and the residue was redissolved in CH$_2$Cl$_2$. The solution was filtered through a glass wool plug. The solution was layered first with toluene then with pentane. After several days, a large amount of red powder formed. The solid material was collected by filtration and washed with pentane to give the desired diiron complex (45.6 mg, 37%). Crystals suitable for X-ray diffraction studies were obtained by layering a solution of complex in CH$_2$Cl$_2$ and

THF with pentane. IR (KBr): ν 3049, 2954, 2924, 2854, 1942, 1713, 1666, 1601, 1579, 1545, 1428, 1389, 1320, 1203, 1186, 1147, 1095, 1004, 883, 840, 788, 736, 702, 632, 542 cm^{-1}. Anal. Calcd for $C_{70}H_{44}F_2Fe_2N_2O_9S \cdot (CH_2Cl_2)_{1.5}$: 62.86; H, 3.47; N, 2.05; Found: C, 63.20; H, 3.53; N, 1.94%. mp (decomp) = 244.1 °C.

[Fe$_2$(F$_2$PIM)(Ph$_3$CCO$_2$)$_2$] (15). In an anaerobic drybox, solid H$_2$F$_2$PIM (51.5 mg, 0.075 mmol) and Ph$_3$CCO$_2$H (43.2 mg, 0.15 mmol) were dissolved in 3.0 mL of THF. A 2.0 mL solution of THF containing [Fe$_2$(Mes)$_4$] (44.1 mg, 0.075 mmol) was added to the reaction vessel, and the mixture was stirred for 1 h. The dark red solution was evaporated to dryness, and the residue was redissolved in toluene. The solution was filtered through a glass wool plug and layered with pentane. Red crystals formed over several days. The solid material was collected by filtration and washed with pentane to give the desired diiron complex (81.0 mg, 76%). Crystals suitable for X-ray diffraction studies were obtained with the same method. IR (KBr): ν 3053, 3027, 2927, 2854, 1950, 1878, 1804, 1597, 1588, 1553, 1448, 1376, 1329, 1203, 1186, 1147, 1000, 840, 788, 732, 699, 546 cm^{-1}. Anal. Calcd for $C_{80}H_{56}F_2Fe_2N_2O_9S$: C, 70.08; H, 4.12; N, 2.04. Found: C, 69.10; H, 4.07; N, 1.95%. mp (decomp) = 176.1 °C.

[Fe$_2$(PIMIC4)(o-Ph$_2$PC$_6$H$_4$CO$_2$)(MeCN)] (16). In an anaerobic drybox, solid H$_3$PIMIC4 (80.0 mg, 0.080 mmol) and o-Ph$_2$PC$_6$H$_4$CO$_2$H (24.5 mg, 0.080 mmol) were dissolved in 3.0 mL of THF. A 2.0 mL solution of THF containing [Fe$_2$(Mes)$_4$] (47.1 mg, 0.080 mmol) was added to the reaction vessel, and the mixture was stirred for 1 h. The crystallization was performed as described above for **6**. The solid material was collected by filtration and washed with pentane to give the desired diiron complex (78.5 mg, 67%). Crystals suitable for X-ray diffraction studies were obtained by layering a solution of the complex in CH$_2$Cl$_2$ with MeCN. IR (KBr): ν 3053, 2958, 2919, 2850, 1579, 1540, 1424, 1406, 1255, 1086, 1043, 1025, 866, 836, 797, 745, 693, 563 cm^{-1}. Anal. Calcd for $C_{84}H_{70}F_2Fe_2N_3O_7P \cdot (CH_2Cl_2)_{0.5}$: C, 69.68; H, 4.91; N, 2.88. Found: C, 69.56; H, 4.49; N, 2.84%. mp (decomp) = 276.1 °C.

[Fe$_2$(PIMIC4)(o-PhSC$_6$H$_4$CO$_2$)(MeCN)] (17). In an anaerobic drybox, solid H$_3$PIMIC4 (100.0 mg, 0.10 mmol) and o-PhSC$_6$H$_4$CO$_2$H (23.0 mg, 0.10 mmol) were dissolved in 4.0 mL of THF. A 3.0 mL solution of THF containing [Fe$_2$(Mes)$_4$] (58.8 mg, 0.10 mmol) was added to the reaction vessel, and the mixture was stirred for 1 h. The crystallization was performed as described above for **6**. The solid material was collected by filtration and washed with pentane to give the desired diiron complex (108.0 mg, 78%). Crystals suitable for X-ray diffraction studies were obtained by layering a solution of the complex in CH$_2$Cl$_2$ with MeCN. IR (KBr): ν 3053, 2954, 2902, 2859, 1601, 1584, 1545, 1424, 1402, 1337, 1281, 1203, 1181, 1000, 840, 788, 740, 697, 672, 538 cm^{-1}. Anal. Calcd for $C_{78}H_{65}F_2Fe_2N_3O_7S \cdot CH_3CN \cdot (CH_2Cl_2)_{0.3}$: C, 68.66; H, 4.92; N, 3.99. Found: C, 68.69; H, 4.77; N, 3.91%. mp (decomp) = 255.6 °C.

[Fe$_2$(PIMIC4)(o-Ph$_2$CHC$_6$H$_4$CO$_2$)(MeCN)] (18). In an anaerobic drybox, solid H$_3$PIMIC4 (50.0 mg, 0.050 mmol) and o-Ph$_2$CHC$_6$H$_4$CO$_2$H (14.4 mg, 0.050 mmol) were dissolved in 2.0 mL of THF. A 1.5 mL solution of THF containing [Fe$_2$(Mes)$_4$] (29.4 mg, 0.050 mmol) was added to the reaction vessel, and the mixture was stirred for 1 h. The crystallization was performed as described above for **6**. The solid material was collected by filtration and washed with pentane to give the desired diiron complex (46.0 mg, 64%). Crystals suitable for X-ray diffraction studies were obtained by layering a solution of the complex in CH$_2$Cl$_2$ with MeCN. IR (KBr): ν 3054, 3023, 2950, 2859, 1601, 1584, 1550, 1424, 1403, 1333, 1286, 1200, 1187, 1001, 836, 789, 750, 694, 672, 538 cm^{-1}. Anal. Calcd for $C_{85}H_{71}F_2Fe_2N_3O_7 \cdot (CH_3CN)_{3.5} \cdot (CH_2Cl_2)_{0.2}$: C, 71.13; H, 5.30; N, 5.85. Found: C, 71.04; H, 4.99; N, 5.87%. mp (decomp) = 304.6 °C.

■ ASSOCIATED CONTENT

Ⓢ Supporting Information

The Supporting Information is available free of charge on the ACS Publications website at DOI: 10.1021/acs.inorg-chem.7b01418.

General procedures and methods, experimental procedures and spectral data for the ligands, details of electrochemical studies, refinement details for the crystal structures, and experimental procedures for reactivity studies (PDF)

Accession Codes

CCDC 1550662−1550675 contain the supplementary crystallographic data for this paper. These data can be obtained free of charge via www.ccdc.cam.ac.uk/data_request/cif, or by emailing data_request@ccdc.cam.ac.uk, or by contacting The Cambridge Crystallographic Data Centre, 12 Union Road, Cambridge CB2 1EZ, UK; fax: +44 1223 336033.

■ AUTHOR INFORMATION

Corresponding Author

*E-mail: lippard@mit.edu. (S.J.L.)

ORCID

Fang Wang: 0000-0002-9192-6858
Sabine Becker: 0000-0001-6618-7259
Andrei Loas: 0000-0001-5640-1645
Stephen J. Lippard: 0000-0002-2693-4982

Author Contributions

The manuscript was written through contributions of all authors. All authors have given approval to the final version of the manuscript.

Notes

The authors declare no competing financial interest.

■ REFERENCES

(1) Wallar, B. J.; Lipscomb, J. D. Dioxygen Activation by Enzymes Containing Binuclear Non-Heme Iron Clusters. *Chem. Rev.* **1996**, *96*, 2625−2657.

(2) Lawton, T. J.; Rosenzweig, A. C. Methane-Oxidizing Enzymes: An Upstream Problem in Biological Gas-to-Liquids Conversion. *J. Am. Chem. Soc.* **2016**, *138*, 9327−9340.

(3) Rosenzweig, A. C.; Nordlund, P.; Takahara, P. M.; Frederick, C. A.; Lippard, S. J. Geometry of the Soluble Methane Monooxygenase Catalytic Diiron Center in Two Oxidation States. *Chem. Biol.* **1995**, *2*, 409−418.

(4) Stubbe, J. A. Protein Radical Involvement in Biological Catalysis? *Annu. Rev. Biochem.* **1989**, *58*, 257−285.

(5) Reichard, P. From RNA to DNA, Why So Many Ribonucleotide Reductases? *Science* **1993**, *260*, 1773−1777.

(6) Logan, D. T.; Su, X.-D.; Åberg, A.; Regnström, K.; Hajdu, J.; Eklund, H.; Nordlund, P. Crystal Structure of Reduced Protein R2 of Ribonucleotide Reductase: The Structural Basis for Oxygen Activation at a Dinuclear Iron Site. *Structure* **1996**, *4*, 1053−1064.

(7) Högbom, M.; Huque, Y.; Sjöberg, B.-M.; Nordlund, P. Crystal Structure of the Diiron/Radical Protein of Ribonucleotide Reductase from Corynebacterium ammoniagenes. *Biochemistry* **2002**, *41*, 1381−1389.

(8) He, C.; Mishina, Y. Modeling Non-Heme Iron Proteins. *Curr. Opin. Chem. Biol.* **2004**, *8*, 201−208.

(9) Reisner, E.; Telser, J.; Lippard, S. J. A Planar Carboxylate-Rich Tetrairon(II) Complex and Its Conversion to Linear Triiron(II) and Paddlewheel Diiron(II) Complexes. *Inorg. Chem.* **2007**, *46*, 10754−10770.

(10) Marchetti, F.; Marchetti, F.; Melai, B.; Pampaloni, G.; Zacchini, S. Synthesis and Reactivity of Haloacetato Derivatives of Iron(II) Including the Crystal and the Molecular Structure of [Fe-(CF$_3$COOH)$_2$(μ-CF$_3$COO)$_2$]$_n$. *Inorg. Chem.* **2007**, *46*, 3378−3384.

(11) Do, L. H.; Lippard, S. J. Evolution of Strategies to Prepare Synthetic Mimics of Carboxylate-Bridged Diiron Protein Active Sites. *J. Inorg. Biochem.* **2011**, *105*, 1774−1785.

(12) Do, L. H.; Lippard, S. J. Toward Functional Carboxylate-Bridged Diiron Protein Mimics: Achieving Structural Stability and Conformational Flexibility Using a Macrocyclic Ligand Framework. *J. Am. Chem. Soc.* **2011**, *133*, 10568−10581.

(13) Minier, M. A.; Lippard, S. J. ^{19}F NMR Study of Ligand Dynamics in Carboxylate-Bridged Diiron(II) Complexes Supported by a Macrocyclic Ligand. *Dalton Trans.* **2015**, *44*, 18111−18121.

(14) Mudadu, M. S.; Singh, A. N.; Thummel, R. P. Preparation and Study of 1,8-Di(pyrid-2′-yl)carbazoles. *J. Org. Chem.* **2008**, *73*, 6513−6520.

(15) Wang, X.; Zhao, L.; Shao, S.; Ding, J.; Wang, L.; Jing, X.; Wang, F. Poly(spirobifluorene)s Containing Nonconjugated Diphenylsulfone Moiety: Toward Blue Emission Through a Weak Charge Transfer Effect. *Macromolecules* **2014**, *47*, 2907−2914.

(16) Klose, A.; Solari, E.; Floriani, C.; Chiesi-Villa, A.; Rizzoli, C.; Re, N. Magnetic Properties Diagnostic for the Existence of Iron(II)-Iron(II) Bonds in Dinuclear Complexes Which Derive from Stepwise Insertion Reactions on Unsupported Iron−Aryl Bonds. *J. Am. Chem. Soc.* **1994**, *116*, 9123−9135.

(17) Robin, M. B.; Day, P. Mixed Valence Chemistry-A Survey and Classification. In *Advances in Inorganic Chemistry and Radiochemistry*; Eleméus, H. J., Sharpe, A. G., Eds.; Academic Press: New York, 1968; Vol. 10, pp 247−422.

(18) Bott, A. W. The Study of Multiple Electron Transfer Reactions by Cyclic Voltammetry. *Curr. Sep.* **1997**, *16*, 61−66.

(19) Fenton, D. E.; Schroeder, R. R.; Lintvedt, R. L. A Unique Two-Electron, Reversible Reduction of a Binuclear Copper(II) Complex. Observation of the Electrochemical Behavior Predicted by Polcyn and Shain for the Sequential Transfer of Two Electrons at the Same Potential. *J. Am. Chem. Soc.* **1978**, *100*, 1931−1932.

(20) Geiger, W. E.; Atwood, C. G.; Chin, T. T. One- and Two-Electron Oxidations of Bimetallic Fulvalene Complexes Studied by Voltammetry and IR Spectroelectrochemistry. In *Molecular Electrochemistry of Inorganic, Bioinorganic and Organometallic Compounds*; Pombeiro, A. J. L., McCleverty, J. A., Eds.; Springer: Dordrecht, Netherlands, 1993; Vol. 385, pp 519−532.

(21) Silva, K. E.; Elgren, T. E.; Que, L., Jr.; Stankovich, M. T. Electron Transfer Properties of the R2 Protein of Ribonucleotide Reductase from *Escherichia coli*. *Biochemistry* **1995**, *34*, 14093−14103.

(22) Liu, K. E.; Lippard, S. J. Redox Properties of the Hydroxylase Component of Methane Monooxygenase from *Methylococcus capsulatus* (Bath). Effects of Protein B, Reductase, and Substrate. *J. Biol. Chem.* **1991**, *266*, 12836−12839.

(23) Paulsen, K. E.; Liu, Y.; Fox, B. G.; Lipscomb, J. D.; Münck, E.; Stankovich, M. T. Oxidation-Reduction Potentials of the Methane Monooxygenase Hydroxylase Component from *Methylosinus trichosporium* OB3b. *Biochemistry* **1994**, *33*, 713−722.

(24) Brown, H. C.; McDaniel, D. H.; Häfliger, O. Dissociation Constants A2. In *Determination of Organic Structures by Physical Methods*; Braude, E. A., Nachod, F. C., Eds.; Academic Press: New York, 1955; Vol. 1, pp 567−662.

(25) Liler, M. Reaction Mechanisms in Sulphuric Acid Solutions. In *Organic Chemistry*; Blomquist, A. T., Ed.; Elsevier: London, England, 1971; Vol. 23, pp 167−305.

(26) Baik, M.-H.; Friesner, R. A. Computing Redox Potentials in Solution: Density Functional Theory as a Tool for Rational Design of Redox Agents. *J. Phys. Chem. A* **2002**, *106*, 7407−7412.

(27) Lord, R. L.; Schultz, F. A.; Baik, M.-H. Two-Electron Redox Energetics in Ligand-Bridged Dinuclear Molybdenum and Tungsten Complexes. *Inorg. Chem.* **2010**, *49*, 4611−4619.

(28) Kryatov, S. V.; Rybak-Akimova, E. V.; Schindler, S. Kinetics and Mechanisms of Formation and Reactivity of Non-Heme Iron Oxygen Intermediates. *Chem. Rev.* **2005**, *105*, 2175−2226.

(29) Bryliakov, K. P.; Talsi, E. P. Active Sites and Mechanisms of Bioinspired Oxidation with H_2O_2, Catalyzed by Non-Heme Fe and Related Mn Complexes. *Coord. Chem. Rev.* **2014**, *276*, 73−96.

(30) Bauschlicher, C. W., Jr.; Langhoff, S. R. Bond Dissociation Energies for Substituted Polycyclic Aromatic Hydrocarbons and Their Cations. *Mol. Phys.* **1999**, *96*, 471−476.

(31) McMillen, D. F.; Golden, D. M. Hydrocarbon Bond Dissociation Energies. *Annu. Rev. Phys. Chem.* **1982**, *33*, 493−532.

(32) Roth, J. P.; Yoder, J. C.; Won, T.-J.; Mayer, J. M. Application of the Marcus Cross Relation to Hydrogen Atom Transfer Reactions. *Science* **2001**, *294*, 2524−2526.

(33) Zhao, M.; Helms, B.; Slonkina, E.; Friedle, S.; Lee, D.; DuBois, J.; Hedman, B.; Hodgson, K. O.; Fréchet, J. M. J.; Lippard, S. J. Iron Complexes of Dendrimer-Appended Carboxylates for Activating Dioxygen and Oxidizing Hydrocarbons. *J. Am. Chem. Soc.* **2008**, *130*, 4352−4363.

(34) Díaz-Torres, R.; Alvarez, S. Coordinating Ability of Anions and Solvents Towards Transition Metals and Lanthanides. *Dalton Trans.* **2011**, *40*, 10742−10750.

(35) Reisner, E.; Abikoff, T. C.; Lippard, S. J. Influence of Steric Hindrance on the Core Geometry and Sulfoxidation Chemistry of Carboxylate-Rich Diiron(II) Complexes. *Inorg. Chem.* **2007**, *46*, 10229−10240.

(36) Arends, I. W. C. E.; Ingold, K. U.; Wayner, D. D. M. A Mechanistic Probe for Oxygen Activation by Metal Complexes and Hydroperoxides and Its Application to Alkane Functionalization by $[Fe^{III}Cl_2tris(2\text{-pyridinylmethyl})amine]^+BF_4^-$. *J. Am. Chem. Soc.* **1995**, *117*, 4710−4711.

(37) MacFaul, P. A.; Ingold, K. U.; Wayner, D. D. M.; Que, L., Jr. A Putative Monooxygenase Mimic Which Functions via Well-Disguised Free Radical Chemistry. *J. Am. Chem. Soc.* **1997**, *119*, 10594−10598.

(38) MacFaul, P. A.; Arends, I. W. C. E.; Ingold, K. U.; Wayner, D. D. M. Oxygen Activation by Metal Complexes and Alkyl Hydroperoxides. Applications of Mechanistic Probes to Explore the Role of Alkoxyl Radicals in Alkane Functionalization. *J. Chem. Soc., Perkin Trans. 2 (1972-1999)* **1997**, 135−145.

(39) Foster, T. L.; Caradonna, J. P. Fe^{2+}-Catalyzed Heterolytic RO−OH Bond Cleavage and Substrate Oxidation: A Functional Synthetic Non-Heme Iron Monooxygenase System. *J. Am. Chem. Soc.* **2003**, *125*, 3678−3679.

(40) Yang, S. J.; Nam, W. Water-Soluble Iron Porphyrin Complex-Catalyzed Epoxidation of Olefins with Hydrogen Peroxide and *tert*-Butyl Hydroperoxide in Aqueous Solution. *Inorg. Chem.* **1998**, *37*, 606−607.

(41) Nam, W.; Han, H. J.; Oh, S.-Y.; Lee, Y. J.; Choi, M.-H.; Han, S.-Y.; Kim, C.; Woo, S. K.; Shin, W. New Insights into the Mechanisms of O−O Bond Cleavage of Hydrogen Peroxide and *tert*-Alkyl Hydroperoxides by Iron(III) Porphyrin Complexes. *J. Am. Chem. Soc.* **2000**, *122*, 8677−8684.

(42) Shin, J. W.; Bae, J. M.; Kim, C.; Min, K. S. Catalysis and Molecular Magnetism of Dinuclear Iron(III) Complexes with *N*-(2-Pyridylmethyl)-Iminodiethanol/-ate. *Dalton Trans.* **2014**, *43*, 3999−4008.